Biological Cybernetics (2019) 113:139–148
https://doi.org/10.1007/s00422-018-0765-y

Biological Cybernetics

ORIGINAL ARTICLE

Optimizing SGLT inhibitor treatment for diabetes with chronic kidney diseases

Anita T. Layton[1]

Received: 4 January 2018 / Accepted: 16 June 2018 / Published online: 28 June 2018

Abstract
Diabetes induces glomerular hyperfiltration, affects kidney function, and may lead to chronic kidney diseases. A novel therapeutic treatment for diabetic patients targets the sodium–glucose cotransporter isoform 2 (SGLT2) in the kidney. SGLT2 inhibitors enhance urinary glucose, Na^+ and fluid excretion and lower hyperglycemia in diabetes by inhibiting Na^+ and glucose reabsorption along the proximal convoluted tubule. A goal of this study is to predict the effects of SGLT2 inhibitors in diabetic patients with and without chronic kidney diseases. To that end, we applied computational rat kidney models to assess how SGLT2 inhibition affects renal solute transport and metabolism when nephron population are normal or reduced (the latter simulates chronic kidney disease). The model predicts that SGLT2 inhibition induces glucosuria and natriuresis, with those effects enhanced in a remnant kidney. The model also predicts that the Na^+ transport load and thus oxygen consumption of the S3 segment are increased under SGLT2 inhibition, a consequence that may increase the risk of hypoxia for that segment. To protect the vulnerable S3 segment, we explore dual SGLT2/SGLT1 inhibition and seek to determine the optimal combination that would yield sufficient urinary glucose excretion while limiting the metabolic load on the S3 segment. The model predicts that the optimal combination of SGLT2/SGLT1 inhibition lowers the oxygen requirements of key tubular segments, but decreases urine flow and Na^+ excretion; the latter effect may limit the cardiovascular protection of the treatment.

Keywords Diabetes · Glucose · Sodium · Metabolism

1 Introduction

In mammals, the kidneys are organs that extract waste from blood and regulate the balance of water, electrolytes, and acid–base species. The kidneys accomplish these crucial tasks by filtering blood through the nephrons. Nephrons are elongated tubules surrounded by a layer of epithelial cells. A portion of the blood supplied to the nephrons is extracted from the bloodstream and directed into the renal tubules. As the extracted fluid flows through the nephrons, its composition constantly changes, as water and solutes are selectively reabsorbed or secreted, depending on the animal's needs. The final fluid that emerges is urine. When renal function is impaired and the kidneys fail to filter properly, waste accumulates in the blood, in a condition called azotemia. If the disease progresses, symptoms such as vomiting, nausea, weight loss, itching, bone damage, etc. become noticeable.

Chronic kidney diseases (CKD) are a growing public health and economic burden. In the USA, one in 10 adults, or more than 20 million, have some levels of CKD. In 2013, CKD patients incurred almost $50 billion in Medicare expenditures. High blood pressure and diabetes are the main causes of CKD [9]. Almost half of individuals with CKD also have diabetes and/or self-reported cardiovascular disease. But despite intense research, the underlying mechanisms that

Communicated by Mette Olufsen.

This research was supported in part by the National Institutes of Health: National Institute of Diabetes and Digestive and Kidney Diseases, Grant R01DK106102 and by the Natural Sciences and Engineering Research Council of Canada (NSERC).

This article belongs to the Special Issue on *Control Theory in Biology and Medicine*. It derived from a workshop at the Mathematical Biosciences Institute, Ohio State University, Columbus, OH, USA.

✉ Anita T. Layton
anita.layton@uwaterloo.ca

[1] Department of Applied Mathematics, University of Waterloo, Waterloo, Ontario, Canada

lead to the development of CKD remain incompletely understood.

There is consensus that renal hypoxia is an important pathway in the development of CKD. In general, renal hypoxia is due to a mismatch between changes in renal oxygen delivery and oxygen consumption (Q_{O2}) [8]. Renal oxygen delivery is primarily determined by renal blood flow [8]. Renal Q_{O2} is mainly driven by the metabolic work of tubular sodium reabsorption, which in turn is largely driven by the filtered load of sodium, and thus glomerular filtration rate (GFR) [7]. It is believed that renal Q_{O2} increases in diabetes, and, without compensatory increases in oxygen supply, renal hypoxia and eventually CKD develops. Thus, one approach to slow progression to CKD in diabetic patients is to reduce or at least limit the increase in renal Q_{O2}.

Under physiological conditions, virtually all filtered glucose is reabsorbed by the kidney, specifically by the proximal tubule, where secondary active transport of sugar is mediated by the Na^+–glucose cotransporter SGLT2. In diabetes, the filtered glucose load may exceed the transport capacity of the proximal tubule, and glucose appears in urine (i.e., glucosuria). Insulin is a popular approach to lower blood glucose level in diabetes, but it has side effects such as weight gain and becomes ineffective in diabetic patients who are insulin resistant. A new alternate approach is to inhibit glucose reabsorption in the kidney, by primarily targeting the early proximal tubule. SGLT2 inhibitors have proven to be effective not only in lowering blood sugar level, but they have also been reported to reduce blood pressure and protect from heart failure, even in patients with CKD and reduced GFR [26,33].

However, inhibition of SGLT2 lowers proximal tubule uptake of not only glucose but Na^+ as well, thereby shifting Na^+ transport to downstream nephron segments. This is unfortunate because the transport efficiency of those downstream segments is lower than the proximal tubule, i.e., those downstream segments require more oxygen to transport the same amount of Na^+ compared to the proximal tubule. This downstream shift of Na^+ transport may be a particular concern, given the potential role of tissue hypoxia in the development of diabetic nephropathy. Thus, a reasonable question is: *Does SGLT2 inhibition have the detrimental effect of lowering medullary oxygen tension* (P_{O2})*?* Two nephron segments that are most vulnerable to hypoxic injury are the S3 segment (or, the proximal straight tubule, which follows immediately the proximal convoluted tubule and expresses the SGLT1) and the medullary thick ascending limb segment. Their vulnerability is due to their location in regions of the medulla that have low baseline P_{O2}, and to their relatively limited capacity for anaerobic metabolism. Thus, an important question is: *To what extent does SGLT2 inhibition increase* Q_{O2} *of the S3 segment and the thick ascending limb?*

An alternative therapeutic approach is dual SGLT1-SGLT2 inhibition. Inhibition of SGLT1 may be a double-edged sword: it protects the S3 segment by reducing its Na^+ transport and thus Q_{O2}, but may further aggravate the thick ascending limb by elevating its transport. Thus, key questions are: *What is the optimal combination of SGLT1 and SGLT2, in terms of suppressing tubular glucose uptake and maintaining a sufficiently high medullary* P_{O2}*? And how would these answers differ between a diabetic patient with healthy kidneys, and one suffering from chronic kidney diseases?*

To address these questions, we have developed computational models of solute transport and metabolism in the kidney of a diabetic control rat (healthy kidney) and a diabetic rat with a remnant kidney (representing CKD). We applied the models to determine Q_{O2} under SGLT2 inhibition and differing combinations of SGLT2 and SGLT1 inhibition.

Modeling methodology

Model simulations were performed using our published models of epithelial transport along nephrons in the kidney of a diabetic control rat and a diabetic rat with CKD (or, remnant kidneys) [22,27]. The nephron model accounts for 15 solutes: Na^+, K^+, Cl^-, HCO_3^-, H_2CO_3, CO_2, NH_3, NH_4^+, HPO_4^{2-}, $H_2PO_4^-$, H^+, HCO_2^-, H_2CO_2, urea, and glucose. The model is formulated for steady state and predicts luminal fluid flow, hydrostatic pressure, luminal fluid solute concentrations, and, with the exception of the descending limb segment, cytosolic solute concentrations, membrane potential, and transcellular and paracellular fluxes.

To compute transcellular and paracellular solute and water fluxes, the model represents the epithelial cells as distinct compartments, with the apical and basolateral members separating the cell from lumen and the interstitium, respectively. The lateral innerspace (i.e., the paracellular pathway between adjacent cells) is explicitly represented. Cell type varies along the nephron. Thus, the set of transporters represented on the apical and basolateral members also vary along the nephron. The model nephron with its distinct segments, and the model proximal tubule epithelial cell is shown in Fig. 1. Submodels for transporters that are essential for this study are described below. Details for other cell models and transporter models can be found in Refs. [29,30] and the references therein.

Diabetes induces renal hypertrophy, hyperfiltration, and alterations in transporter expression. As in our previous model [30], we simulate diabetic conditions by simultaneously raising plasma glucose, single-nephron glomerular filtration rate (SNGFR), tubular diameter and length, and the expression levels of SGLT2 and other selected Na^+ transporters, and by decreasing SGLT1 expression. Details on changes in transporter expression can be found in Ref. [30]. The same diabetes-induced fractional changes in transporter expression are assumed in control and remnant kidneys (see below). Plasma glucose concentration is taken to be 25 mM in

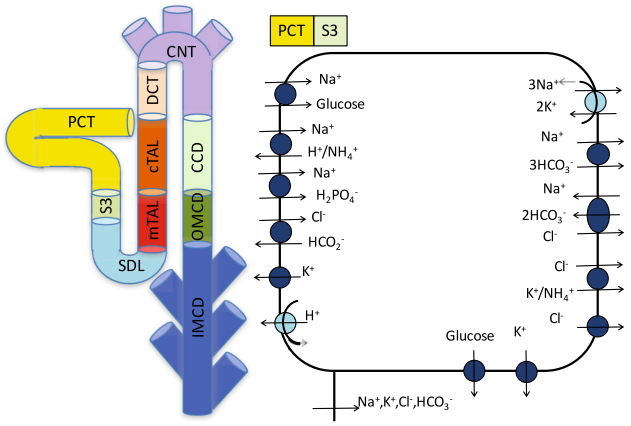

Fig. 1 Schematic diagrams of the model nephron (left) and the proximal tubule epithelial cell (right). *PCT* proximal convoluted tubule, *SDL* short descending limb, *mTAL/cTAL* medullary/cortical thick ascending limb, *DCT* distal convoluted tubule, *CNT* connecting tubule, *CCD* cortical collecting duct, *OMCD/IMCD* outer/inner-medullary collecting duct

control and slightly higher at 30 mM in remnant kidneys [32]. Model parameters under baseline conditions can be found in Refs. [22,23,28–30].

1.1 Glucose transport

Given that the focus of this study on diabetes and glucose excretion, we describe below glucose transport by the proximal tubule, mediated by SGLT1 and SGLT2 on the apical membrane, and by glucose transporter (GLUT) on the basolateral membrane.

The fluxes of glucose and Na^+ across SGLT1 (on the apical membrane of the S3 epithelial cells, Fig. 1) are computed using the kinetic model developed by [6,36]. The 6-state model assumes a Na^+:glucose stoichiometry of 2:1, does not assume rapid binding to the transporter, and includes 14 rate constants. Flux equations and parameter values can be found in Refs. [36,47].

The kinetic behavior of SGLT2 (on the apical membrane of the proximal convoluted cells, Fig. 1) is relatively less well characterized. Based upon the sodium-alanine cotransporter model [14], the SGLT2 flux is calculated as

$$J_{\text{glu}}^{\text{SGLT2}} = \frac{X_{\text{SGLT2}} k_u^f}{\Phi}\left(C_{\text{glu}}^{\text{lum}} C_{\text{Na}^+}^{\text{lum}} \exp(\zeta) - C_{\text{glu}}^{\text{cyt}} C_{\text{Na}^+}^{\text{cyt}}\right) \quad (1)$$

$$J_{\text{Na}^+}^{\text{SGLT2}} = J_{\text{glu}}^{\text{SGLT2}} \quad (2)$$

where

$$\zeta = F(\Psi_{\text{lum}} - \Psi_{\text{cyt}})/(RT)$$

$$n^{\text{lum}} = \frac{C_{\text{Na}^+}^{\text{lum}}}{K_{m,\text{Na}^+}^{\text{SGLT2}}}, \quad n^{\text{cyt}} = \frac{C_{\text{Na}^+}^{\text{cyt}}}{K_{m,\text{Na}^+}^{\text{SGLT2}}}$$

$$g^{\text{lum}} = \frac{C_{\text{glu}}^{\text{lum}}}{K_{m,\text{glu}}^{\text{SGLT2}}}, \quad g^{\text{cyt}} = \frac{C_{\text{glu}}^{\text{cyt}}}{K_{m,\text{glu}}^{\text{SGLT2}}}$$

$$\Phi = (1 + n^{\text{lum}} + g^{\text{lum}} + n^{\text{lum}} g^{\text{lum}})(1 + n^{\text{cyt}} g^{\text{cyt}}) + (1 + n^{\text{cyt}} + g^{\text{cyt}} + n^{\text{cyt}} g^{\text{cyt}})(1 + n^{\text{lum}} g^{\text{lum}} \exp(\zeta)) \quad (3)$$

X_{SGLT2} characterizes the density of SGLT2 transporters, k_u^f is the forward translocation rate of the unloaded carrier, $C_{\text{glu}}^{\text{lum}}$ and $C_{\text{Na}^+}^{\text{lum}}$, respectively, denote the luminal concentration of glucose and Na^+, $C_{\text{glu}}^{\text{cyt}}$ and $C_{\text{Na}^+}^{\text{cyt}}$ denote the cytosolic concentration of glucose and Na^+, and Ψ_{lum} and Ψ_{cyt} represent the electric potential in the lumen and cytosol. R is the ideal gas constant, F is the Faraday constant, and T is the temperature. Lastly, $K_{m,\text{glu}}^{\text{SGLT2}}$ and $K_{m,\text{Na}^+}^{\text{SGLT2}}$, respectively, denote the binding affinity of SGLT2 to glucose and Na^+. Equation 1 posits a simultaneous mechanism for the transport of Na^+ and glucose. It also assumes that (a) the binding affinities to a given ion on the luminal and cytosolic sides of the membrane are the same, (b) the forward (k_u^f) and backward (k_u^b) translocation rates of the unloaded carrier, and the backward translocation rate of the fully loaded carrier (k_l^b), are all equal, and (c) the forward translocation rate of the fully loaded carrier (k_l^f) is given by $(k_u^f k_l^b / k_u^b) \cdot \exp(\zeta)$, so as to satisfy thermodynamics constraints (i.e., the principle of microscopic reversibility).

The flux of glucose across GLUT transporters is determined based on the Maki and Keiser model [31]

$$J_{\text{glu}}^{\text{GLUT}} = V_m^{\text{GLUT}}\left(\frac{K_m^{\text{GLUT}}(C_{\text{glu}}^{\text{cyt}} - C_{\text{glu}}^{\text{ext}})}{(K_m^{\text{GLUT}} + C_{\text{glu}}^{\text{cyt}})(K_m^{\text{GLUT}} + C_{\text{glu}}^{\text{ext}})}\right) \quad (4)$$

where V_m^{GLUT} is the maximum glucose flux, K_m^{GLUT} is the glucose dissociation equilibrium constant, and $C_{\text{glu}}^{\text{ext}}$ denotes the external (peritubular) glucose concentration.

Parameter values for glucose transport are listed in Table 1. The expression levels of SGLT1 and SGLT2, and the SGLT2 binding constants are chosen so that (a) the fraction of the glucose load that is reabsorbed by the S3 segment during SGLT2 inhibition is consistent with experimental measurements in mice [38], and (b) glucosuria begins when plasma glucose reaches $\sim$ 16 mM (see below).

1.2 Oxygen consumption

The measurements of Welch et al. suggest that, in rats, the whole kidney basal-to-total Q_{O2} ratio is 25–30% [46]. By extrapolation, Evans et al. estimated that this ratio ranges between $\sim$ 10 and 45% in rats under normal conditions (i.e., with $FE_{Na} = 1\%$) [7]. We assume here that, in the absence of

Table 1 Glucose transport parameters

Parameter	Value	References
SGLT1 density	83.3×10^{-9} mmol cm^{-2}	[28]
SGLT2 transport rate, $X_{\mathrm{SGLT2}} k_u^f$	1.30×10^{-3}cm^4 mmol^{-1} s^{-1}	[28]
SGLT2 binding affinity to glucose, $K_{\mathrm{m,glu}}^{\mathrm{SGLT2}}$	4.9 mM	[28]
SGLT2 binding affinity to sodium, $K_{\mathrm{m,Na^+}}^{\mathrm{SGLT2}}$	25 mM	[28]
GLUT1 maximum rate, $V_{\mathrm{m}}^{\mathrm{GLUT1}}$	3.00×10^{-6} mmol s^{-1} cm^{-2}	[28]
GLUT1 affinity to glucose, K_m^{GLUT1}	2.0 mM	[31]
GLUT2 maximum rate, V_m^{GLUT2}	1.625×10^{-6} mmol s^{-1} cm^{-2}	[28]
GLUT2 affinity to glucose, K_m^{GLUT2}	17 mM	[31]
Tight junction permeability to glucose	3.1×10^{-6} cm/s	[13]

diabetes, Q_{O2}^{basal*} remains constant and equal to 20% of total Q_{O2} under baseline conditions. That is

$$Q_{O2}^{basal*} = 0.20(Q_{O2}^{basal} + Q_{O2}^{active*}) = (0.20/0.80)\,Q_{O2}^{active*} \tag{5}$$

where Q_{O2}^{active} is the rate of Q_{O2} for active Na^+ reabsorption, and the asterisk denotes base-case conditions. To account for the higher basal Q_{O2} in diabetic rats [16,34,35], as in our previous study [30], Q_{O2}^{basal} is taken to increase (relative to the non-diabetic Q_{O2}^{basal*}) by 40% in all cortical segments and by 160% each in the S3 segment and medullary collecting duct, and to remain unchanged in the medullary thick ascending limb.

In turn, Q_{O2}^{active} is determined based upon the ATP consumption of the basolateral Na, K-ATPase. Oxidative metabolism yields about 5 moles of ATP per mole of O_2 consumed, depending on the substrate [37]. Furthermore, 1 mole of ATP is required to pump out 3 moles of Na^+ via the Na,K-ATPase. Diabetes decreases the $T_{Na}^{active}/Q_{O2}^{active}$ ratio in the proximal tubule by 20%, as a result of increased fatty acid metabolism [1]. We thus have

$$Q_{O2}^{active} = T_{Na}^{active}/12 \tag{6}$$

where T_{Na}^{active} is the rate of Na^+ transport across Na,K-ATPase pumps. Note that T_{Na}^{active} differs from the overall rate of Na^+ reabsorption (denoted T_{Na}), as a significant fraction of Na^+ is passively transported across the paracellular pathway.

1.3 Simulating a remnant kidney

Because CKD typically involves loss of nephrons, we use the remnant kidney as a model for CKD. Specifically, we simulate the kidney in a 5/6-nephrectomized (5/6-NX) rat, i.e., one in which 5/6 of its renal mass has been surgically removed. Following nephrectomy, the remaining nephrons can adapt with appropriately elevated urinary excretion per nephron to maintain total excretion rates. Such compensatory response involves adaptive changes in GFR, in tubular growth, and in transepithelial transport. Following our previous approach to this setting [22], we assumed in 5/6-NX that SNGFR was increased by 110 and 50% in the superficial and juxtamedullary nephrons, respectively, [15]. Additional model parameters for simulating a remnant kidney can be found in [22].

1.4 Simulating SGLT2 inhibition

SGLT2 inhibition was found to lower blood glucose levels by 60% in diabetic Akita mice, from ~25 to 10 mM, without altering the renal membrane expression of SGLT1 nor that of SGLT2 (i.e., the diabetes-induced changes were maintained) [44]. Thus, in simulating SGLT2 blockade in diabetic control rats, we reduced the plasma concentration of glucose to 10 mM, in addition to decreasing SNGFR from diabetic levels. Because filtered glucose load was lower in nephrectomized rats, glucouria and thus the glucosuric efficacy of SGLT2 inhibitors were reduced as well. Thus, we assumed that SGLT2 inhibition in diabetic CKD lowered plasma glucose concentration to 20 mM.

Furthermore, SGLT2 inhibition is known to reduce or prevent diabetic-induced hyperfiltration in rodents [43–45] and humans [4], via its effects on renal tubular reabsorption (a feedback and tubular hydrostatic pressure effect) and possibly also by lowering the effects of high blood glucose levels on vascular tone (an effect not attributable to a feedback mechanism in the kidney known as tubuloglomerular feedback (TGF) [2]). Thus, when simulating the effects of SGLT2 inhibition in diabetic rats, we lowered SNGFR half-way to its value in non-diabetic rats; that is, if $\mathrm{SNGFR}_{\mathrm{non-diabetic}}$ and $\mathrm{SNGFR}_{\mathrm{diabetes}}$ denote SNGFR in non-diabetic and diabetic rats, respectively, then under SGLT2 inhibition, SNGFR is set to

$$0.5 \times (\mathrm{SNGFR}_{\mathrm{non-diabetic}} + \mathrm{SNGFR}_{\mathrm{diabetes}})$$

We assumed that in SGLT2 inhibition, systemic application of the inhibitor reaches the entire proximal tubule

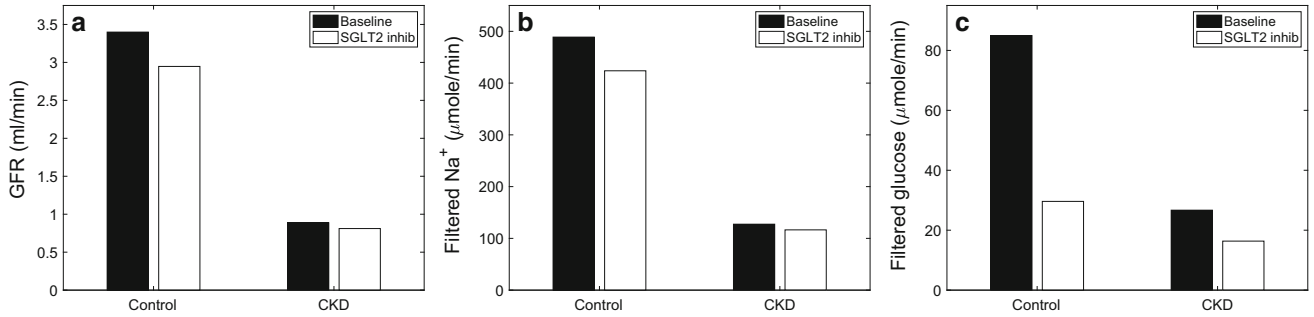

Fig. 2 GFR (**a**), filtered Na^+ (**b**), and filtered glucose (**c**), given per animal, with or without CKD or SGLT2 inhibition. A reduction in nephron number lowers the total filtered rates of fluid (GFR), Na^+, and glucose

from Bowman space downward. Thus, we abolished transport across SGLT2 by 100%. Furthermore, in wild-type mice, chronic inhibition of SGLT2 by empagliflozin was found to reduce SGLT1 protein by 35% [44]. These changes in transporter density were accounted for in our simulations.

2 Simulation results

We considered the kidney of a diabetic control rat and of a diabetic rat with CKD. For each type of kidney, we conducted simulations separately under baseline conditions (i.e., untreated) and with SGLT2 inhibition. GFR and filtered Na^+ and glucose loads are shown in Fig. 2. GFR and filtered loads are lower in the CKD rat due to the reduced nephron population. As previously noted, SGLT2 inhibition reduces GFR via TGF; see Fig. 2a. These GFR-lowering effects are similarly reflected on filtered Na^+ load (Fig. 2b). Furthermore, SGLT2 inhibition in a diabetic kidney lowers plasma glucose concentration from 25 to 10 mM in control, and from 30 mM to 20 mM in CKD; see filtered glucose load in Fig. 2c.

2.1 Effect of SGLT2 inhibition in a diabetic control rat

Because SGLT2 inhibitors are designed to lower blood glucose level, and because glucose is primarily reabsorbed along the proximal tubule, we show predicted proximal tubule luminal glucose flow, obtained with and without SGLT2 inhibition, in Fig. 3a. The model assumes that little glucose is reabsorbed downstream of the proximal tubule. Figure 4 shows the predicted urine flow, Na^+ excretion, and glucose excretion.

In a diabetic control kidney with elevated blood glucose level of 25 mM, 59% of the filtered glucose was predicted to be reabsorbed via SGLT2 along the proximal convoluted tubule under baseline (or, untreated) conditions; see Fig. 3a, solid line. That transport fraction was reduced to 7% of filtered glucose under SGLT2 inhibition (Fig. 3a, dashed line). (Recall that filtered glucose load with SGLT2 inhibition was

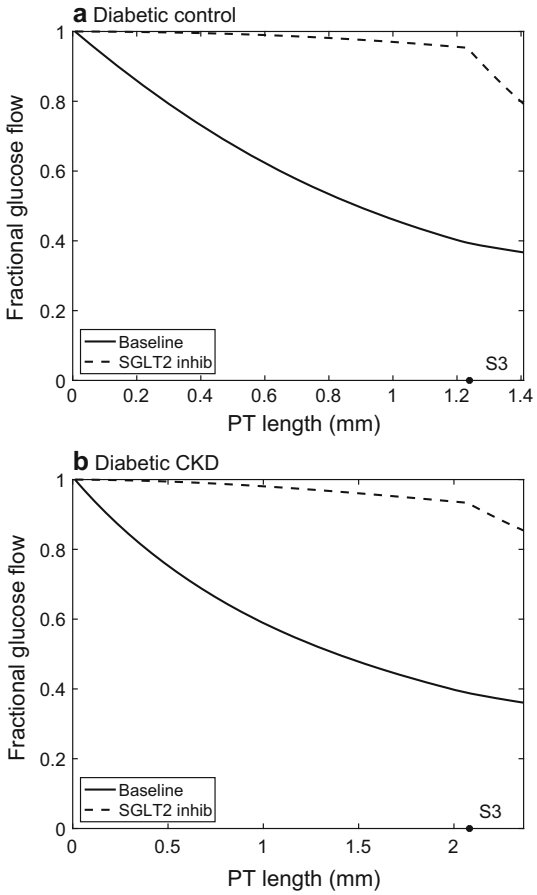

Fig. 3 Predicted proximal tubule glucose flow, obtained for the control (**a**) and CKD (**b**) kidney, with and without SGLT2 inhibition. The proximal tubule (PT) is functionally divided into two segments: the (initial) proximal convoluted tubule and the S3 segment (labeled). The dot denotes the division between these two segments

31% of baseline due to differential effects on GFR and blood glucose; see Fig. 2c). The S3 segment reabsorbed 3% of filtered glucose via SGLT1 under baseline conditions, and 19% of filtered glucose with SGLT2 inhibition (Fig. 3a). In both scenarios, a significant amount of glucose was excreted in

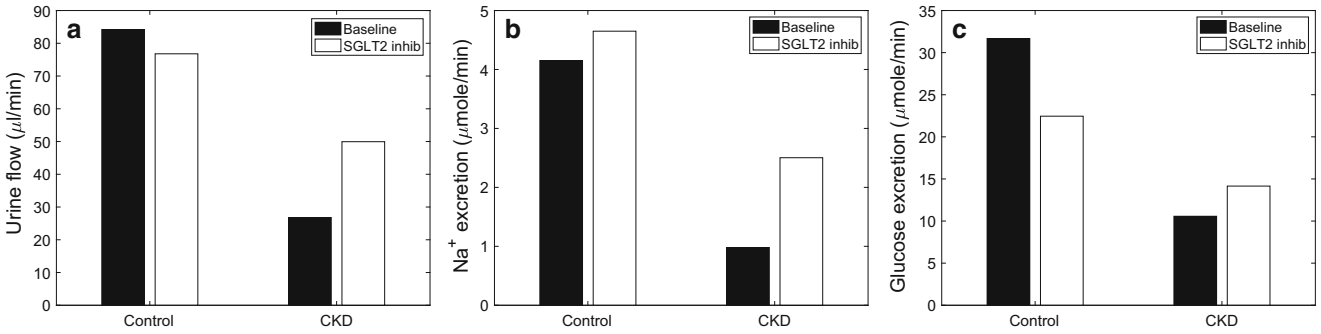

Fig. 4 Predicted urinary flow (**a**), Na^+ excretion (**b**), and glucose excretion (**c**), given per animal, with or without CKD or SGLT2 inhibition

the urine (32 and 22 μmol/min per animal for baseline and SGLT2 inhibition, respectively; Fig. 4c).

In the diabetic control kidney, SGLT2 inhibition raised tubular fluid glucose concentration and thus osmolality sufficiently downstream from the glomerulus, thereby reducing water reabsorption. The higher water content diluted luminal Na^+ concentration and decreased Na^+ reabsorption, particularly via the paracellular pathway. Consequently, SGLT2 inhibition reduced both transcellular and paracellular Na^+ transport along the proximal convoluted tubule; total Na^+ reabsorption along this segment decreased to 78% of baseline. This increased Na^+ delivery to the thick ascending limbs, and as well as Na^+ transport along these segments. Taken together, in diabetic conditions, urinary Na^+ excretion was predicted to increase by 12% with SGLT2 inhibition; see Fig. 4b.

2.2 Effect of SGLT2 inhibition in a diabetic rat with CKD

Plasma glucose concentration in a diabetic rat with CKD following SGLT2 inhibition was assumed to remain higher compared to control (20 versus 10 mM). However, GFR was much reduced; thus, compared to control, the filtered glucose load was lower in CKD (see Fig. 2c). The effects of SGLT2 inhibition in the diabetic remnant kidneys were qualitatively similar to diabetic control. Under SGLT2 inhibition, 7% of the filtered glucose was reabsorbed via SGLT1 along the S3 segment in the diabetic remnant kidney. SGLT2 inhibition lowered GFR. And compared to the glucose excretion rate of 22 μmol/min in control, SGLT2 inhibition yielded a lower excretion rate of 14 μmol/min in CKD.

The effect of SGLT2 inhibition on Na^+ excretion in diabetic CKD was similar to control. SGLT2 inhibition lowered Na^+ reabsorption along the proximal convoluted tubule by 23% (similar to 22% reduction in diabetic control). Along the S3 segment, SGLT2 inhibition increased Na^+ secretion by > 5 fold (compared to the untreated case) in a remnant kidney. This was caused by the reduction in luminal Na^+ concentrations due to strong water retaining effect of the very high amounts of filtered glucose which were delivered to the S3 segment in response to SGLT2 inhibition. (In contrast, net Na^+ reabsorption was maintained along the S3 segment under SGLT2 inhibition in diabetic control.) Along the thick ascending limbs, SGLT2 inhibition increased Na^+ transport by 24% in a remnant kidney. SGLT2 inhibition yielded a much higher fractional increase in Na^+ excretion of 56% (Fig. 4b), compared to 12% in control, due to the decreased Na^+ reabsorption along the proximal convoluted tubule as well as to the increased Na^+ secretion along the S3 segment.

2.3 Effect of SGLT2 inhibition on metabolism

As discussed above, tubular Q_{O2} depends, in part, on transcellular Na^+ transport. SGLT2 inhibition decreases proximal tubule Na^+ reabsorption, thereby increasing Na^+ delivery and Na^+ transport load of downstream segments. In other words, SGLT2 inhibition is expected to shift Na^+ transport to distal segments, which likely elevates their Q_{O2}. Given that some of these segments, such as the S3 segment and medullary thick ascending limb, are vulnerable to hypoxic injury, we determine the Q_{O2} of the proximal convoluted tubule, S3 segment, and medullary thick ascending limb in a control and CKD kidney, with and without SGLT2 inhibition. Results are shown in Fig. 5.

A comparison between panels A (control) and B (CKD) in Fig. 5 indicates that, due to the much elevated SNGFR, transport load and thus Q_{O2} *per nephron* were substantially increased in CKD compared to control (left axis). Note, however, that *whole-kidney* transport and metabolism were lower in CKD (right axis), whose nephron population is only 1/6 of control.

SGLT2 inhibition reduced transcellular Na^+ transport and thus Q_{O2}^{active} along the proximal convoluted tubule of a diabetic kidney, in large part due to a lower GFR. That effect was attenuated by a reduction in nephron number. This was due to the higher plasma glucose concentration, relative to control, assumed in a nephrectomized kidney following SGLT2

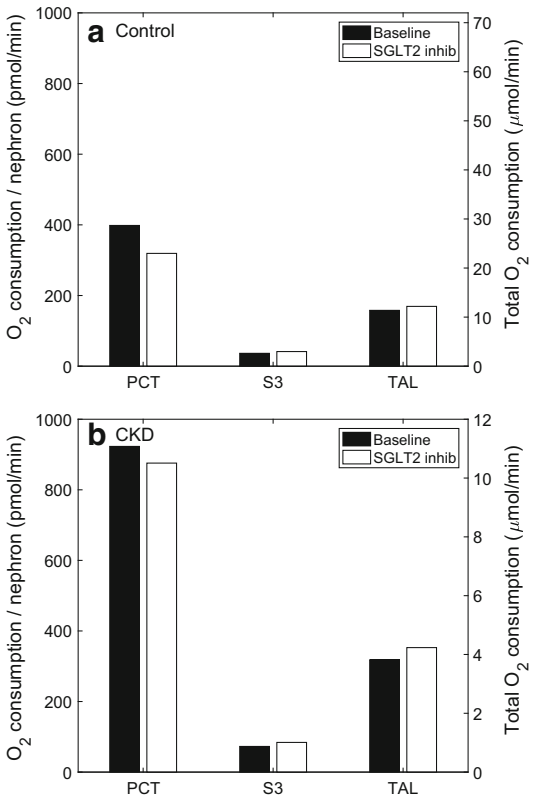

Fig. 5 Total Q_{O2} along key nephron segments obtained for control (**a**) and CKD (**b**) cases, with or without SGLT2 inhibition

inhibition. The resulting higher tubular fluid osmolality led to water retention, lower tubular fluid [Na^+], and, in the CKD case, increased paracellular Na^+ secretion.

An increase in transcellular Na^+ transport was observed along the S3 segment due to enhanced SGLT1-mediated transport. The model predicted that total S3 segmental Q_{O2} increased by 18% with SGLT2 inhibition in the diabetic control kidney. In the diabetic remnant kidney, S3 segmental Q_{O2} increased by 16%. Modest and similar increases in Q_{O2} were predicted along distal segments in diabetic control and remnant kidneys on a single-nephron level (Fig. 5).

2.4 Optimal SGLT2/SGLT1 dual inhibition

Our results above indicate that SGLT2 inhibition may significantly increase the O_2 demand of the S3 segment. Because that segment resides in an O_2-poor region of the kidney, elevating its O_2 requirement, which, without a compensatory increase in O_2 supply, may lead to renal hypoxia. An alternative therapeutic treatment may be dual SGLT2/SGLT1 inhibition. SGLT1 is expressed along the S3 segment, and its inhibition may lower active Na^+ transport and thus metabolic demand of that segment. In part because the S3 segment is much shorter than the proximal convoluted tubule (about 10% in length), SGLT1 inhibition alone cannot sufficiently elevate urinary glucose excretion.

Here the key question is: *What is the optimal combination of SGLT2 and SGLT2 inhibition?* That is, what fractions of SGLT2 and SGLT1 should be inhibited? Ideally, the combined treatment should yield glucose excretion at a level similar to SGLT2 inhibition. If glucose excretion is too low, the drug may not effective in lowering blood glucose level; too high, the patient may suffer from hypoglycemia. Additionally, the combined treatment should lower S3 O_2 requirement without significantly increasing that of the thick ascending limb.

To identify the optimal dual inhibition for diabetic control and CKD rats, we conducted simulations in which SGLT1 was 100% inhibited (for maximum S3 protection), whereas SGLT2 was inhibited at varying degrees, ranging from 90 to 100%. We computed urine flow, Na^+ excretion, and glucose excretion. These results are shown in Fig. 6. For the diabetic control kidney, 100% SGLT1 inhibition paired with 94.6% SGLT2 inhibition yielded the same glucose excretion as 100% SGLT2 inhibition alone; this combination was identified as the *optimal dual treatment*. Compared to 100% SGLT2 inhibition alone, the optimal dual treatment yielded significantly lower Na^+ excretion and urine flow; see Fig. 6a, b, solid curves. For the diabetic remnant kidney, the optimal combination is 100% SGLT1 inhibition paired with 95.7% SGLT2 inhibition; that combination also yielded lower Na^+ excretion and urine flow, although the effect was attenuated compared to control.

We then assessed the effect of dual inhibition on Q_{O2} of the proximal convoluted tubule, S3 segment, and the thick ascending limb. Results are shown in Fig. 7 for the diabetic control and remnant kidneys. The dots correspond to the optimal combinations (identified above), whereas the crosses corresponding to values obtained with 100% SGLT2 inhibition alone. The model predicted that the optimal combined treatment lowered Q_{O2} in all three segments, with the most significant fractional reduction obtained along the S3 segment (77 and 86%, respectively, for the diabetic control and remnant kidneys). Importantly, the model predicted that more Na^+ was reabsorbed with the optimal dual treatment, resulting in lower Na^+ delivery to the thick ascending limbs and lower Q_{O2} along those segments (Fig. 7). In order words, not only does the dual treatment protect the S3 segment from hypoxia, it protects the thick ascending limb as well.

3 Discussion

We have applied a computational model of renal tubular solute transport and metabolism to assess the impact of SGLT2 inhibition on tubular Q_{O2} and urinary excretion in a diabetic control kidney and in a diabetic remnant kidney.

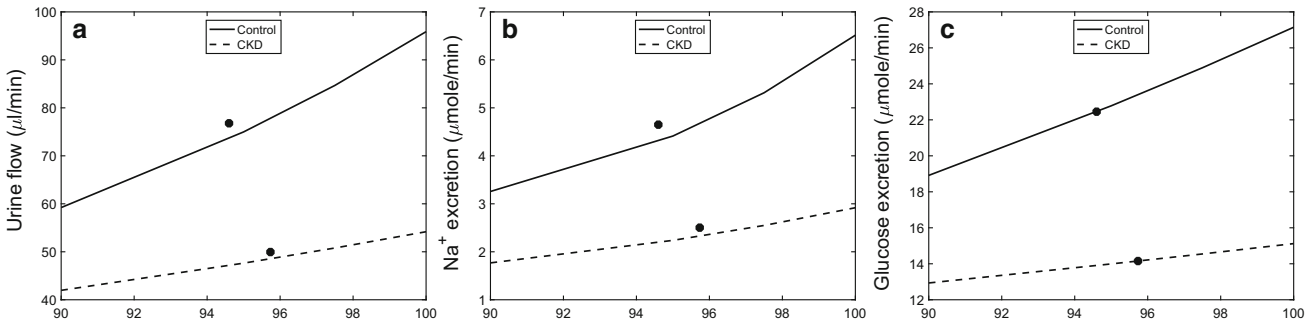

Fig. 6 Urine flow (**a**), Na^+ excretion (**b**), and glucose excretion (**c**) obtained with 100% SGLT1 inhibition and varying degree of SGLT2 inhibition. Results obtained for control and CKD cases. Dots correspond to SGLT2 inhibition that yields the same urinary glucose excretion with only 100% SGLT2 inhibition

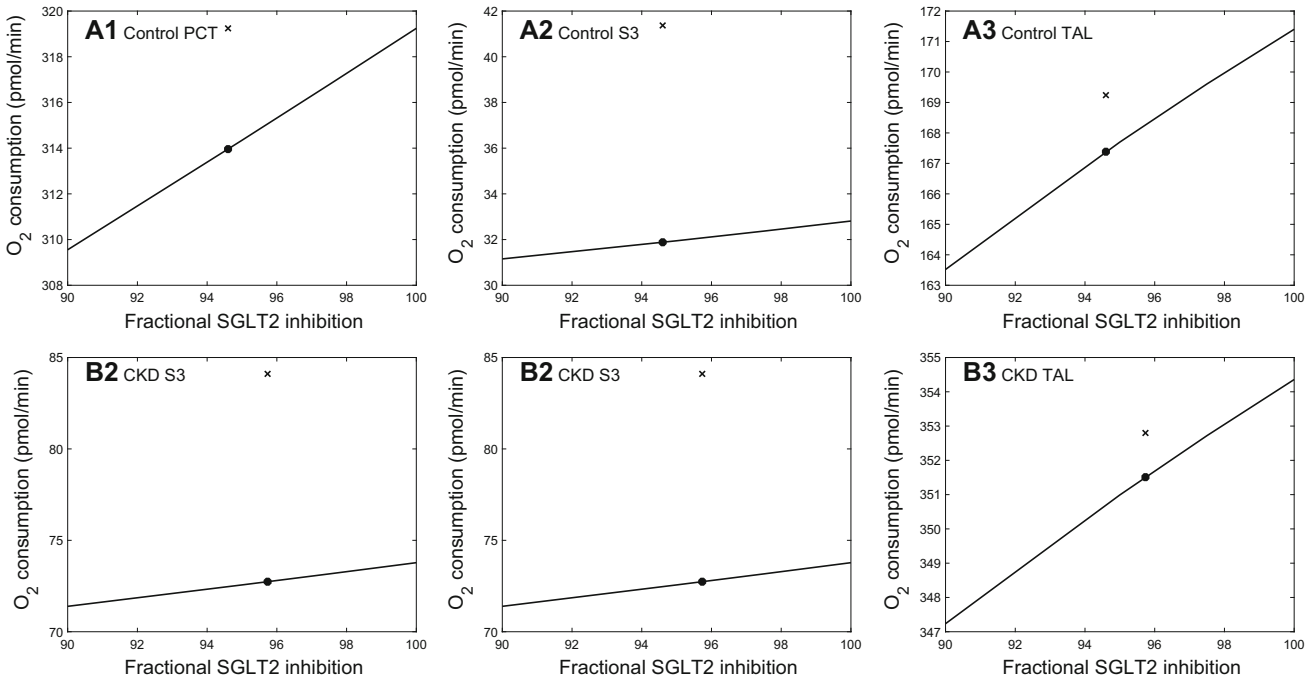

Fig. 7 Segmental Q_{O2} obtained with 100% SGLT1 inhibition and varying degree of SGLT2 inhibition. Results obtained for control and CKD cases. Dots correspond to "optimal" SGLT2 inhibition that yields the same urinary glucose excretion with only 100% SGLT2 inhibition. Crosses corresponding to 100% SGLT2 inhibition only

The model predicted that in a diabetic control kidney, SGLT2 inhibition induces natriuresis (but not diuresis); see Fig. 4. That prediction is consistent with the blood pressure lowering effect observed in patients treated with SGLT2 inhibitors. What is even more interesting is the result for a diabetic remnant kidney. Not only was the natriuretic effect augmented, the model also predicted that SGLT2 inhibition induces diuresis and glucosuria (Fig. 4). This result is consistent with the clinical observation that SGLT2 inhibitors reduce blood pressure and protect from heart failure in patients with chronic kidney diseases and reduced GFR [33].

In both the diabetic control and remnant kidneys, while SGLT2 inhibition lowers O_2 demand along the proximal convoluted tubule, it increases active Na^+ transport and Q_{O2} along the S3 segment and thick ascending limb; see Fig. 5. To protect the vulnerable S3 segment from hypoxic injury, dual SGLT2/SGLT1 inhibitors may be used. We conducted simulations to identify the "optimal combination" for each type of diabetic kidney, such that the predicted glucose excretion matches SGLT2-only inhibition. The model predicted that the optimal combinations lower the Q_{O2} of the proximal convoluted tubule, S3 segment, and the thick ascending limb (Fig. 7). However, urine flow and Na^+ excretion are reduced (Fig. 6), which may limit the cardiovascular-protective effect of the treatment.

The present nephron model predicts cellular solute concentrations, tubular flow, and luminal fluid solute concentrations. Interstitial fluid composition is assumed known *a priori*. As a result, the model does not account for the interactions among nephrons, or the interactions between nephrons and the renal vasculature. Also, in mammals renal blood flow is tightly regulated by a number of autoregulatory mechanisms, such as the tubuloglomerular feedback and myogenic response [20,40,42]; none of these mechanisms are represented in this model. Despite these limitations, the model can be used as an essential component in an integrated model of kidney function: renal blood flow can be predicted by incorporating a model of the afferent arteriole (e.g., [3,5,41]) and a model of the tubuloglomerular feedback (e.g., [17,24,25,39]). Interactions among renal tubule and vessels can be represented by embedding the nephron model into a kidney model (e.g., [18,19,21]). To more accurately assess the risk of hypoxia, one may want to predict tissue P_{O2} under differing pathophysiologic and therapeutic conditions. That can be achieved by incorporating the present model into a kidney model that represents, in addition to the many solutes already included in the nephron models, oxygen, nitric oxide (NO), and superoxide (O_2^-) (e.g., [10–12]).

References

1. Baines A, Ho P (2002) Glucose stimulates O_2 consumption, NOS, and Na/H exchange in diabetic rat proximal tubules. Am J Physiol Renal Physiol 283:F286–F293
2. Carmines P, Ohishi K, Ikenaga H (1996) Functional impairment of renal afferent arteriolar voltage-gated calcium channels in rats with diabetes mellitus. J Clin Invest 98(11):2564–2571
3. Chen J, Sgouralis I, Moore L, Layton H, Layton A (2011) A mathematical model of the myogenic response to systolic pressure in the afferent arteriole. Am J Physiol Renal Physiol 300:F669–F681
4. Cherney D, Perkins B, Soleymanlou N, Maione M, Lai V, Lee A, Fagan N, Woerle H, Johansen O, Broedl U, von Eynatten M (2014) Renal hemodynamic effect of sodium–glucose cotransporter 2 inhibition in patients with type 1 diabetes mellitus. Circulation 129:587–597
5. Edwards A, Layton A (2014) Calcium dynamics underlying the afferent arteriole myogenic response. Am J Physiol Renal Physiol 306:F34–F48
6. Eskandari S, Wright E, Loo D (2005) Kinetics of the reverse mode of the Na^+/glucose cotransporter. J Membr Biol 204:23–32
7. Evans R, Harrop G, Ngo J, Ow C, O'Connor P (2014) Basal renal oxygen consumption and the efficiency of oxygen utilization for sodium reabsorption. Am J Physiol Renal Physiol 306:F551–F560
8. Evans R, Ince C, Joles J, Smith D, May C, O'Connor P, Gardiner B (2013) Haemodynamic influences on kidney oxygenation: the clinical implications of integrative physiology. Clin Exp Pharmacol Physiol 40:106–122
9. Foley R, Collins A (2007) End-stage renal disease in the United States: an update from the United States Renal Data System. J Am Soc Nephrol 18:2644–2648
10. Fry B, Edwards A, Layton A (2015) Impacts of nitric oxide and superoxide on renal medullary oxygen transport and urine concentration. Am J Physiol Renal Physiol 308:F967–F980
11. Fry B, Edwards A, Layton A (2015) Impact of nitric-oxide-mediated vasodilation and oxidative stress on renal medullary oxygenation: a modeling study. Am J Physiol Renal Physiol 310:F237–F247
12. Fry B, Edwards A, Sgouralis I, Layton A (2014) Impact of renal medullary three-dimensional architecture on oxygen transport. Am J Physiol Renal Physiol 307:F263–F272
13. Garvin J (1990) Glucose absorption by isolated perfused rat proximal straight tubules. Am J Physiol Renal Physiol 259:F580–F586
14. Jauch P, Lauger P (1986) Electrogenic properties of the sodium-alanine cotransporter in pancreatic acinar cells: II. Comparison with transport models. J Membr Biol 94:117–127
15. Kim S, Heo N, Jung J, Son MJ, Jang H, Lee J, Oh Y, Na K, Joo K, Han J (2010) Changes in the sodium and potasssium transporters in the course of chronic renal failure. Nephron Physiol 115:31–41
16. Körner A, Eklöf AC, Celsi G, Aperia A (1994) Increased renal metabolism in diabetes: mechanism and functional implications. Diabetes 43:629–633
17. Layton A (2010) Feedback-mediated dynamics in a model of a compliant thick ascending limb. Math Biosci 228:185–194
18. Layton A (2011) A mathematical model of the urine concentrating mechanism in the rat renal medulla: I. Formulation and base-case results. Am J Physiol Renal Physiol 300:F356–F371
19. Layton A (2011) A mathematical model of the urine concentrating mechanism in the rat renal medulla: II. Functional impliciations of three-dimensional architecture. Am J Physiol Renal Physiol 300:F372–F394
20. Layton A (2015) Recent advances in renal hemodynamics: insights from bench experiments and computer simulations. Am J Physiol Renal Physiol 308:F951–F955
21. Layton A, Dantzler W, Pannabecker T (2012) Urine concentrating mechanism: impact of vascular and tubular architecture and a proposed descending limb urea-Na^+ cotransporter. Am J Physiol Renal Physiol 302:F591–F605
22. Layton A, Edwards A, Vallon V (2017) Adaptive changes in GFR, tubular morphology and transport in subtotal nephrectomized kidneys: modeling and analysis. Am J Physiol Renal Physiol 313:F199–F209
23. Layton A, Laghmani K, Vallon V, Edwards A (2016) Solute transport and oxygen consumption along the nephrons: effects of Na^+ transport inhibitors. Am J Physiol Renal Physiol 311:F1217–F1229
24. Layton A, Moore L, Layton H (2006) Multistability in tubuloglomerular feedback and spectral complexity in spontaneously hypertensive rats. Am J Physiol Renal Physiol 291:F79–F97
25. Layton A, Moore L, Layton H (2009) Multistable dynamics mediated by tubuloglomerular feedback in a model of coupled nephrons. Bull Math Biol 71:515–555
26. Layton A, Vallon V (2018) Cardiovascular benefits of SGLT2 inhibition in diabetes and chronic kidney diseases. Acta Physiol 222:e13050
27. Layton A, Vallon V (2018) SGLT2 inhibition in a kidney with reduced nephron number: modeling and analysis of solute transport and metabolism. Am J Physiol Renal Physiol 313:F969–F984
28. Layton A, Vallon V, Edwards A (2015) Modeling oxygen consumption in the proximal tubule: effects of NHE and SGLT2 inhibition. Am J Physiol Renal Physiol 308(12):F1343–F1357
29. Layton A, Vallon V, Edwards A (2016) A computational model for simulating solute transport and oxygen consumption along the nephron. Am J Physiol Renal Physiol 311:F1378–F1390
30. Layton A, Vallon V, Edwards A (2016) Predicted consequences of diabetes and SGLT inhibition on transport and oxygen consumption along a rat nephron. Am J Physiol Renal Physiol 310(11):F1269–F1283
31. Maki L, Keizer J (1995) Mathematical analysis of a proposed mechanism for oscillatory insulin secretion in perfused HIT-15 cells. Bull Math Bioll 57:569–591

32. O'Donnell M, Kasiske B, Daniels F, Keane W (1986) Effects of nephron loss on glomerular hemodynamic and morphology and diabetic rats. Diabetes 35:1011–1015
33. Oliva R, Bakris G (2014) Blood pressure effects of sodium-glucose co-transport 2 (SGLT2) inhibitors. J Am Soc Hypertens 8:330–339
34. Palm F, Cederberg J, Hansell P, Liss P, Carlsson P (2003) Reactive oxygen species cause diabetes-induced decrease in renal oxygen tension. Diabetologia 46:1153–1160
35. Palm F, Hansell P, Ronquist G, Waldenstrom A, Liss P, Carlsson P (2004) Polyol-pathway-dependent disturbances in renal medullary metabolism in experimental insulin-deficient diabetes mellitus in rats. Diabetologia 47:1223–1231
36. Parent L, Supplisson S, Loo D, Wright E (1992) Electrogenic properties of the cloned Na^+/glucose cotransporter: II. A transport model under nonrapid equilibrium conditions. J Membr Biol 125:63–79
37. Rich P (2003) The molecular machinery of Keilin's respiratory chain. Biochem Soc Trans 6:1095–1105
38. Rieg T, Masuda T, Gerasimova M, Mayoux E, Platt K, Powell D, Thomson S, Koepsell H, Vallon V (2014) Increase in SGLT1-mediated transport explains renal glucose reabsorption during genetic and pharmacological SGLT2 inhibition in euglycemia. Am J Physiol Renal Physiol 306:F188–F193
39. Ryu H, Layton A (2012) Effect of tubular inhomogeneities on feedback-mediated dynamics of a model of a thick ascending limb. Med Math Biol 30:191–212
40. Sgouralis I, Layton A (2014) Theoretical assessment of renal autoregulatory mechanisms. Am J Physiol Renal Physiol 306:F1357–F1371
41. Sgouralis I, Layton A (2012) Autoregulation and conduction of vasomotor responses in a mathematical model of the rat afferent arteriole. Am J Physiol Renal Physiol 303:F229–F239
42. Sgouralis I, Layton A (2015) Mathematical modeling of renal hemodynamics in physiology and pathophysiology. Math Biosci 264:8–20
43. Thomson S, Rieg T, Miracle C, Mansoury H, Whaley J, Vallon V, Singh P (2012) Acute and chronic effects of SGLT2 blockade on glomerular and tubular function in the early diabetic rat. Am J Physiol Regul Int Comp Physiol 302:R75–R83
44. Vallon V, Gerasimova M, Rose M, Masuda T, Satriano J, Mayoux E, Koepsell H, Thomson S, Rieg T (2014) SGLT2 inhibitor empagliozin reduces renal growth and albuminuria in proportion to hyperglycemia and prevents glomerular hyperltration in diabetic Akita mice. Am J Physiol Renal Physiol 306:194–204
45. Vallon V, Rose M, Gerasimova M, Satriano J, Platt K, Koepsell H, Cunard R, Sharma K, Thomson S, Rieg T (2013) Knockout of Na-glucose transporter SGLT2 attenuates hyperglycemia and glomerular hyperfiltration but not kidney growth or injury in diabetes mellitus. Am J Physiol Renal Physiol 304:F156–F167
46. Welch WJ, Baumgartl H, Lubber D, Wilcox C (2001) Nephron pO2 and renal oxygen usage in the hypertensive rat kidney. Kidney Int. 59:230–237
47. Wright E, Loo D, Hirayama B (2011) Biology of human sodium glucose transporters. Physiol Rev 91:733–794